Materials Today: Proceedings 93 (2023) 24–30

Contents lists available at ScienceDirect

Materials Today: Proceedings

journal homepage: www.elsevier.com/locate/matpr

# Anti-icing solutions combining printed electronics and nanotexturing of Al alloys

Olatz Adarraga [a,*], Celina Vaquero [a], Leire Bilbao [a], Jon Maudes [a], Ana Pérez-Márquez [a], Haizea Villaverde [a], Izaskun Bustero [a], Ibai Santamaría [a], Marie-Laure Pervier [b]

[a] Tecnalia Basque Research and Technology Alliance (BRTA), P Mikeletegi 2, Donostia-San Sebastian 20009, Spain
[b] Cranfield University, Centre of Propulsion and Thermal Power Engineering, School of Aerospace, Transport and Manufacturing, College road, Cranfield MK43 0AL, UK

ARTICLE INFO

*Article history:*
Available online 26 May 2023

*Keywords:*
Superhydrophobic
Printed Heater
Anti-icing
Carbon PTC inks

ABSTRACT

Aluminum superhydrophobic (SHP) surfaces have been prepared by the combination of chemical micro-texturing and surface functionalization with long-chained polyfluoroalkyl moieties. On the opposite side to the modified surface self-limiting heating element has been printed using carbon based possitive temperature coefficient (PTC) inks. Different heater configurations were tested to optimize heater design. Results showed that the combination of both strategies was able to maintain the aluminum surface ice free under tested conditions. The developed hybrid system showed good performance under anti-icing conditions with potential to be applied in aircraft systems.
Copyright © 2023 Elsevier Ltd. All rights reserved.
Selection and peer-review under responsibility of the scientific committee of the International Conferences & Exhibition on Nanotechnologies, Organic Electronics & Nanomedicine-Nanotexnology 2022.

## 1. Introduction

Low power consumption ice protection solutions are needed for aeronautics (e.g.: Leading edges), automotive and many other sectors (construction, energy infrastructures, etc..) resulting in less generator load and more reserve for other systems. Ice protection strategies (active or passive) can be generally classified into anti-icing or de-icing. Anti-icing systems keep the surface to be protected (aircraft wing for instance) completely ice free requiring continuous energy consumption. In de-icing systems ice build-ups are allowed to form (during off-time of the active system) to get periodical shed by air stream via melting (active) or detaching ice from the surface of the wing due to low surface free energy (passive).

Active solutions based on thermoelectrical strategies are a good option for ice protection systems especially for future all-electric vehicles. For large components in aeronautics, a combination of both strategies, de-icing and anti-icing, is required. Periodically heated strips (de-icing) are used to shed the accreted ice regularly. Permanently heated areas (anti-icing) are used to evaporate moisture into the atmosphere as soon as it touches the surface, for which evaporation temperature needs to be reached. Combining de-icing heated strips together with anti-icing strips on stagnation line to prevent ice bridging and chordwise parting strips, the surface to be protected is splitted into smaller areas. This way the shed of ice is finally carried away by the air stream during in-flight conditions [1].

Some electrical heating systems consist of electrical heating elements embedded inside the membrane or laminated on the surface. Heating pads of this type usually consist of an electrically conductive material in contact with the wire or other metal heating elements dispersed throughout the conductive layer sandwiched between two insulation layers. Electrical energy for the heating elements used in aeronautics is derived from a generating source driven by one or more of the aircraft engines. The electrical energy is continuously supplied possibly requiring high power supply for anti-icing or de-icing performance.

*Abbreviations:* PTC, Possitive Temperature Coefficient; SHP, Superhydrophobic; SAM, Self-Assembled Monolayer; WCA, Water Contact Angle; HCA, Hexadecane Contact Angle; CIWT, Cranfield Icing Wind Tunnel; LWC, Liquid Water Content; MVD, Median Volume Diameter.

* Corresponding authors.
*E-mail address:* Olatz.Adarraga@tecnalia.com (O. Adarraga).

https://doi.org/10.1016/j.matpr.2023.05.337
2214-7853/Copyright © 2023 Elsevier Ltd. All rights reserved.
Selection and peer-review under responsibility of the scientific committee of the International Conferences & Exhibition on Nanotechnologies, Organic Electronics & Nanomedicine-Nanotexnology 2022.

In recent years, several alternative systems have been proposed, which attempt to improve the power efficiency and operational effectiveness of anti-icing or de-icing systems. Printed heaters based on carbon resistive materials show great potential to impart efficient anti/de-icing properties to structural components [2]. Printable positive temperature coefficient (PTC) carbon inks showing self-limiting performance exhibit a positive resistance change with an increase in temperature. When power is applied, the resistance increases and limits the electrical current to the heater, requiring less energy than traditional carbon printed technologies. At a certain temperature, an equilibrium is reached leading to self-regulating heaters. Moreover, PTC inks with self-limiting temperature are formulated to rapidly heat to a specific threshold temperature ("switch-off temperature") and then maintain constant temperature for the device.

In the last decade, passive anti-icing and de-icing solutions based on reducing ice-affinity of system through surface functionalization are also attracting much interest in different research fields. Passive anti-icing protections such as superhydrophobic (SHP) and icephobic coatings, can be potentially employed to prevent the ice adhesion and its growth [3]. The surface free energy reduction would reduce ice adhesion strength making it easier to remove ice from the surface and reducing ice accretion. However, the complex nature of ice creates many challenges when designing ice repellent surfaces. SHP surfaces are considered a viable passive anti-icing method as they can delay freezing time, even though they cannot avoid icing completely under real ice conditions. However, SHP surfaces can help in active de-icing strategy.

In combination with active anti-icing/de-icing systems, SHP surface would lead to complete water removal from the treated surface to avoid freezing of supercooled sessile droplets, as it is one of the ice formation routes on solid surfaces [4]. Consequently, hybrid methods combining both, active and passive solutions, can greatly improve anti-icing/de-icing efficiency reducing system energy consumption. In such case, the active system would require lower energy, as the melting of a thin ice layer (in contact with the surface) is enough for the passive system, SHP surface, to remove ice under a minimum force (air stream). Several works are published in relation to combination of both strategies. For instance, Zhao et al. [5] worked on sandwich structures for aircraft industry, comparing an electric heating coating system alone with the same combined with a SHP coating, and demonstrated up to 27 % heating power has been saved thanks to superhydrophobicity. Additionally, Gao et al. [6] demonstrated that, in wind turbine instead of using the conventional strategy to resistively heat the entire hydrophilic blade surface, combining SHP and active strategy could keep the entire blade surface ice free with only $\sim$ 10 % of the required power consumption. Antonini et al. [7] demonstrated the effectiveness of a SHP coating strategy to combat ice formation on surfaces exposed to icing condition, reducing heating power on surfaces exposed to ice. A conventional resistor heating system coupled to the leading edge was used for testing. Zhao et al. [8] developed a multi-layered coating on Glass Fibre Reinforced plastic which exhibited excellent conductivity and electric heating properties together with SHP properties, obtaining outstanding energy saving performance in anti-icing/de-icing tests.

In this work anti-icing solutions combining printed PTC ink-based heating element and micro-nanotextured SHP aluminum alloys are fabricated. Two carbon inks with self-limiting temperatures have been considered for the printed heater systems in different configurations. They have been studied in combination with a SHP aluminum alloy surface to study the required power energy to maintain the surface ice free, considering ice conditions at −10 °C. From [1], 6 °C is the minimum temperature to prevent the surface from freezing. In this study a surface constant temperature of 6–10 °C is targeted.

## 2. Material and methods

The substrate material used was 1-mm thick sheet of commercial cold-rolled wrought AA1050 aluminum alloy provided by Alustock S.A. For the SHP treatment HCl (37 %) was purchased from Scharlab and used to prepare 3 M solution in deionized water. Granular mixture of sodium bifluoride and ferric sulfate from Turco Española, S.A. as well as nitric acid (HNO3, purity 67 %) from Sigma-Aldrich (St. Louis, MO, USA) were used to prepare deoxidation bath. Absolute ethanol (99.9 % purity) was purchased from Scharlab S.L. 1H,1H,2H,2H-perfluorodecyltriethoxysilane (FAS17, 97 % purity) was purchased from Sigma-Aldrich. All of them were used as received. Anodizing process of chemically etched AA1050 was carried out by Anesdur S.L. (Ordizia) in sulfuric acid medium according to internal procedures that allowed to obtain coatings which meet the requirements of the MIL-A-8625 TYPE II, CLASS 1 standard.

The microtextured surface processing includes the following steps. First, the AA1050 plates were cleaned in acetone and dried with nitrogen blow. Some areas of the sample were protected with NITO tape in order to avoid etching of the complete surface, only the target area was exposed. Chemical etching was applied by dipping the target area into a 3.0 M HCl solution at room temperature. Then, they were rinsed with deionized water, and dried in a nitrogen blow. At the end, a deoxidation step was applied on the complete sample in an acid bath composed by Fe2(SO4)3 (60–108 g/L) NaHF2 (<12 g/L) and HNO3 (7 g/L) in distilled water at room temperature. Then, they were rinsed in deionized water, and dried with compressed air. Afterwards, a 20 μm thick anodic layer was grown on complete samples. For the SHP treatment, FAS17 was diluted in ethanol solution (1 wt%). For SHP performance the microtextured area of the specimens were dipped during 2 h and cured for 30 min at 100 °C to obtain a self-assembled monolayer (SAM) on the treated AA1050 surface.

SEM microscopy was used to study the microtextured and functionalized surfaces using a low-vacuum JEOL JSM 5910 LV equipment. Secondary electron and backscattered electron images were collected at 20 kV.

The static contact angle (θc) of a drop of a solution over a flat surface of the tested material is measured in the sessile-drop test. Fig. 1 shows a graphical representation of static contact angle and surface tension in the solid–liquid, solid–vapour and liquid–vapour interfaces.

The static contact angle of water, WCA (surface free energy 72.8 mN/m), and hexadecane, HCA (surface free energy 27.5 mN/m), on each microtextured and functionalized specimen were measured using a goniometer (Digidrop MCAT and OCA 15 EC Dataphysics). 20 μL droplets were placed on three different spots on each sample and the image analysis was performed.

The results of the contact angle measurements with the two solutions allowed the calculation of the surface free energy according to the Owens-Wendt method, which considers two types of interaction in a solid–liquid interface. The determination of polar

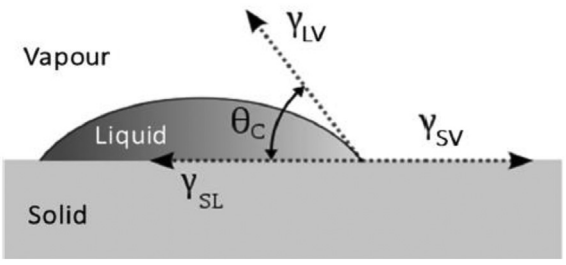



**Fig. 1.** Wet-drop test ($\theta_c$ = contact angle).

and dispersive surface energy components will be calculated from slope ($\sqrt{\gamma_{sv}^{p}}$) and y-intercept ($\sqrt{\gamma_{sv}^{d}}$) of the regression line when plotting $\frac{\gamma_{lv}(1+\cos\theta_c)}{2\sqrt{\gamma_{lv}^{d}}}$ versus $\sqrt{\frac{\gamma_{lv}^{p}}{\gamma_{lv}^{d}}}$, using experimental contact angle data as well as polar and dispersive theoretical surface tension values of each of the test liquids.

(where $\theta_c$ is the contact angle; $\gamma$ is the surface tension; subscripts sl, sv and lv refer to the solid–liquid, solid– vapor and liquid–vapor interfaces, respectively; superscripts d and p refer to dispersive and polar components, respectively).

The potential icephobicity of the samples under screening was evaluated using the mode I test rig in the Cranfield Icing Wind Tunnel (CIWT)Fig. 2.

Ice was grown in the CIWT at a temperature of −10 °C with a tunnel wind speed of 30 m/s, a cloud liquid water content (LWC) of approximatively 1.7 g/m3 and droplets median volume diameter (MVD) of 20 μm.

The substrates consisted of cylinders made of AA2024 onto which a coupon of the material of interest was glued (thermal adhesive). The cylinders have a hole in their center and are screwed onto two bars in the test section as shown in Fig. 2. A plastic disc was placed above the central hole and was held in place using a small suction provided by a vacuum pump. The disc, whose dimension was slightly larger than the hole, acted as a defect to initiate the crack leading to mode I fracture [9].

The tunnel was cooled down at −10 °C and when the temperature was stable, water was sprayed. 12 min were needed to reach a minimum ice thickness of 15 mm at the central part. At which point, gradually increasing pressure was applied on the ice block through the hole at a rate of 10 bar/s to detach the ice.

During the test, the thickness of the ice was visually estimated as well as the type of fracture – adhesive, cohesive or mixed (recorded in percentage of adhesive part). Ice adhesion data were obtained by converting the critical pressure needed to remove the ice from the sample first into fracture energy and then into tensile strength using the equations provided in [9]. The results are provided in term of fracture energy only.

The heating elements have been previously printed and characterized on PET substrate. Two commercial carbon-based inks have been used, Henkel WIK20816-9 and Loctite ECI 8001 with self-regulating temperatures of 40 °C and 65 °C, respectively. Carbon layers of 90x90 mm$^2$ and 15 μm thickness are printed. Silver bus-bars and electrodes with different configurations are printed on top of the carbon layer. Both carbon and silver layers were screen-printed with a semiautomatic screen-printer (EKRA E2) and a PET type screen mesh 77.48. The heating behavior of the printed elements are tested with a thermographic camara (OPTRIS PI160) at 12 V and 24 V. As the resistive heating system is based on Carbon ink, Thermographic camera emissivity has been calibrated for the Carbon layer using a Thermocouple. Emissivity has been adjusted to 0.93. The power consumption is calculated by: P = I*V.

Finally, an aluminum prototype is fabricated (Fig. 3). One of the faces of the sample Fig. 3 (a) has been divided in two different areas: one with SHP treatment (SHP) and the other one with no treatment at all (Bare Al). The objective of this separation is to compare both areas under same heating conditions. On the back surface Fig. 3 (b) a carbon heater was printed on the previously anodized aluminum surface. The silver electrodes were printed on top of the carbon layer. A commercial encapsulant compatible with the carbon ink was screen printed on top of the heater for humidity protection. A sample combining bare aluminum and SHP surface with no heating system on it was included for reference. Both samples were supported at approximately 45° ±10° from the vertical. The active system anti-icing performance has been analyzed in a climatic chamber at −10 °C. Water was periodically sprayed on the samples. In the test the surface temperature was continuously monitored using a thermocouple located on the exposed surface (in the limit between SHP and Bare Al).

## 3. Results and discussion

### 3.1. SHP surface

A SHP aluminum surface is processed in order to reduce surface free energy, allowing, in combination with the printed heater, low energy consumption for the anti-icing active strategy.

Based on previous works of authors [10], an optimized micro-step like structure is produced on the aluminum surface in one single step combined with industrial anodic layers and polyfluoroalkyl (FAS17) functionalization in order to obtain SHP and oleophobic surface (Fig. 4). The micro-step surface structure combined with low surface free energy, processed by FAS17 grafting, leads to SHP surfaces. An intermediate anodizing process produces a 20 μm thick aluminum oxide layer grown conformally on the micro-step structured aluminum surface. This anodic layer helps to improve surface durability, enhancing protection and maintaining superhydrophobicity and oleophobicity on the microtextured aluminum surface under corrosive environment, as demonstrated by authors. Additionally, anodic layer provides better adhesion and, due to the physical and chemical properties of the oxide layer resembling a ceramic, it also provides electrical insulation significantly reducing conductivity compared to untreated aluminum. Consequently, anodic layer processed on the bare aluminum sur-

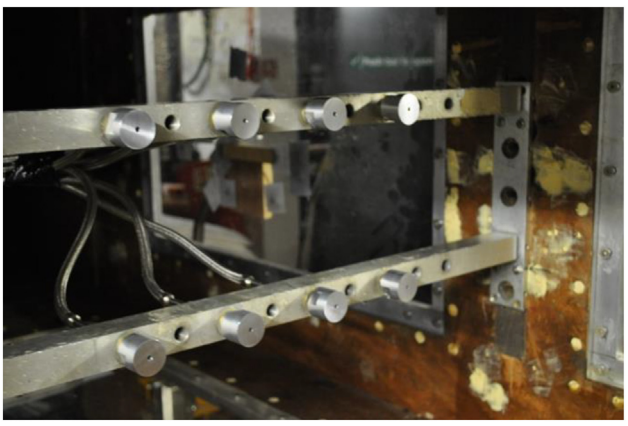


**Fig. 2.** Mode I test in the test section of the CIWT.

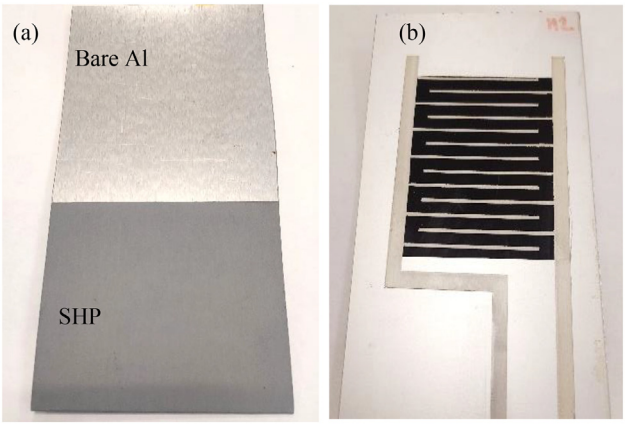



**Fig. 3.** Image of the Hybrid prototype a) SHP and Bare Al surface and b) Heater surface.

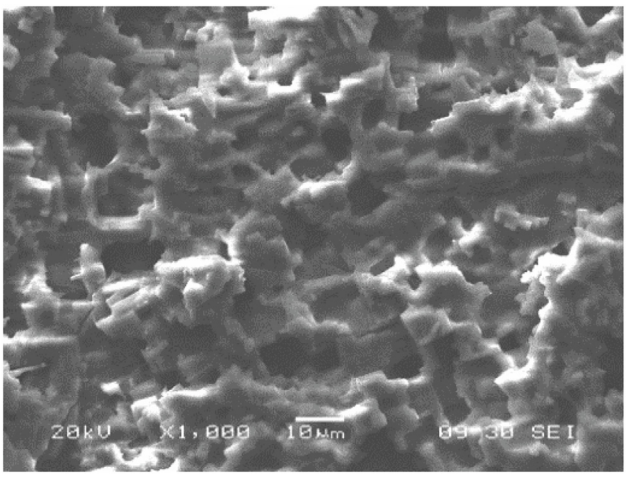



**Fig. 4.** SEM image of SHP surface.

face will also provide insulation and enhance adhesion for printed heater.

AA1050 sample has been partially textured and completely anodized. The microtextured and anodized area has been functionalized through FAS17 grafting producing a SHP and oleophobic surface. The adhesion of both liquids, water and hexadecane, to the substrate on the treated area was characterized qualitatively by the static contact angle. Results are shown in Fig. 5 including Bare Al as reference. It can be observed that the surface was SHP although WCA was not quantitatively measured due to instability of the droplet when contact angle was higher than 140° (droplet not holding on to the surface), resulting in demonstration of the SHP behavior [11]. HCA was also higher than 90° showing oleophobicity.

From contact angle results in Fig. 5 the surface free energy has been calculated using Owens-Wendt method. For polar liquid (water) on SHP surface, 140° was considered for calculations even if actual contact angle may be higher. The resulting total surface free energy is 29.5 mJ/m2 for Bare Al and 1.25 mJ/m2 for SHP, showing that the adhesion strength is very low between solid and liquid in contact for the SHP surface.

The low adhesion energy of SHP aluminum would prevent water droplets impinging on the treated area to stay in the surface contrarily to the bare aluminum surface, facilitating water removal from treated surface. Nevertheless, as widely treated on literature, it is well known that SHP does not necessarily mean icephobic [12]. Indeed, the breaking of the contact between two bodies (being one of them ice and the other one the aluminum substrate) is crucially affected by the interface roughness, necessary to achieve superhydrophobicity [13].

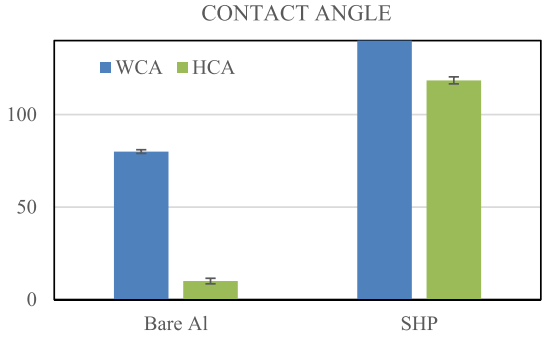



**Fig. 5.** Contact Angle results for water and Hexadecane on Bare Al (left) and SHP (right).

Ice adhesion characterization test results are shown in Table 1. SHP surface shows higher adhesion strength than bare aluminum surface, 1.034 J/m2 for SHP surface while 0.227 J/m2 for bare aluminum. When looking at the results the type of fracture is also important, as SHP surface shows cohesive fracture, i.e. ice layer is internally cracked instead of being adhesively detached from the surface. This means more energy would have been required for ice detachment at the interface. Nevertheless, from these results it can be concluded that the tested SHP surface is not icephobic. Therefore, maintaining liquid state of water is essential for ice removal on these surfaces.

Heating the exposed surface at a target temperature would lead to ice fusion at the interface. The target temperature in this case (where an external temperature of −10 °C is considered) has been considered at approximately 9–10 °C, as already stated in previous section, leading to a thin liquid water layer maintenance in the interface between aluminum and ice, which would lead to an easy removal of the ice due to low surface free energy of SHP surface.

### 3.2. Heating system

A heating system was studied based on two PTC carbon inks and silver ink based interdigit electrodes. To carry out the electrode design selection, one of the PTC inks (self-limiting temperature of 65 °C) was considered and tested. Four different configurations were studied combining: two different electrode designs, COMB (parallel electrodes) and SNAKE (meander electrodes), fixed at two different distances between electrodes 4 mm and 16 mm (Fig. 6).

Fig. 7 shows the temperature reached for the 4 samples at different Voltages. The results showed that 4 mm distance between electrodes for both configurations address to the highest temperatures.

Further testing was carried out with 4 mm distance samples on both configurations SNAKE and COMB. Fig. 8 shows thermograph images at 24 V of both samples. From these thermograph images it can be observed that the SNAKE configuration leads to some cold areas within the heater surface (located between the end of each electrode and the outer electrode line surrounding it). The COMB configuration leads to good temperature homogeneity on the heater surface. Thus, the COMB design with 4 mm distance among electrodes (4COMB) configuration is selected for further study.

The second PTC ink (self-limiting temperature of 40 °C) was tested with the 4COMB design for comparison. Samples were tested to compare the performance of the two PTC inks at different voltages. Fig. 9 shows the heating profile of both inks at 12 V and 24 V (voltage values for common transformers) and the power consumption for the 4COMB configuration. Power consumption is an important factor for active system and consequently it is calculated for both cases. The results showed that both heaters reach the self-limiting temperature in a short time (10–30 s) at 24 V, while at 12 V the self-limiting temperature is not reached in any of them. Thus, 24 V are required for the tested configuration to reach the self-limiting temperature. Lower energy consumption is observed in the case of 40 °C self-limiting ink (5.69 W) compared to the 65 °C self-limiting ink (7.78 W). Consequently, the 40 °C self-limited 4COMB heater is selected for the aluminum prototype to study the temperature reached in an environment of −10 °C.

**Table 1**
Fracture energy and type of fracture of SHP surface and bare Al at −10 °C.

| | Type of fracture | Fracture Energy (J/m2) |
|---|---|---|
| Bare Al | Adhesive | 0.227 ± 0.039 |
| SHP | Cohesive | 1.034 ± 0.260 |

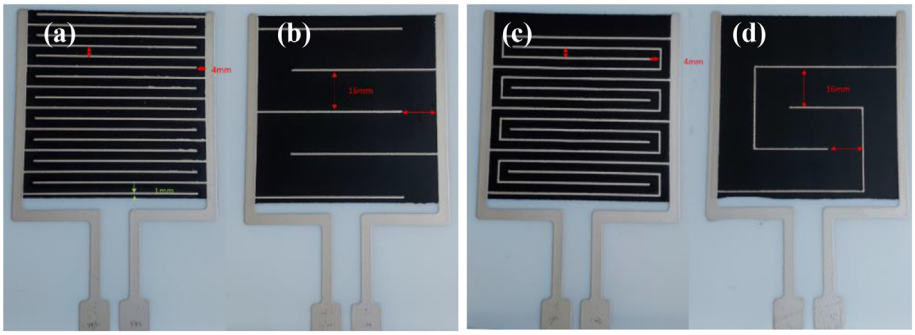



**Fig. 6.** Different configurations of Heater (a) 4COMB (b) 16COMB (c) 4SNAKE and (d) 16SNAKE.

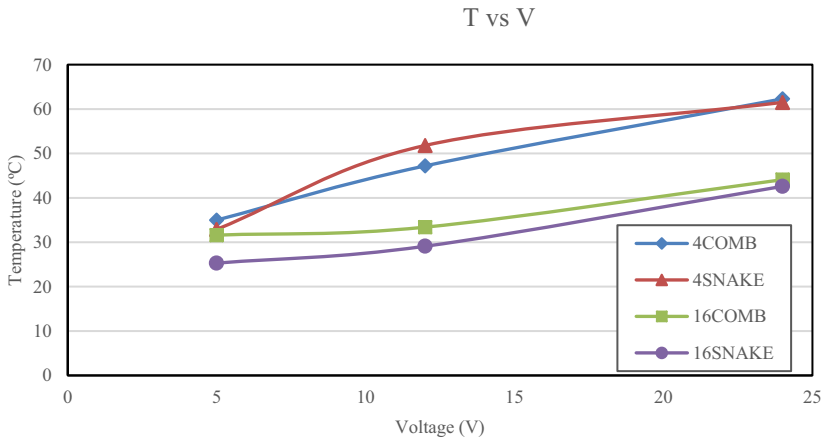



**Fig. 7.** Temperature of the different configurations under different voltages.

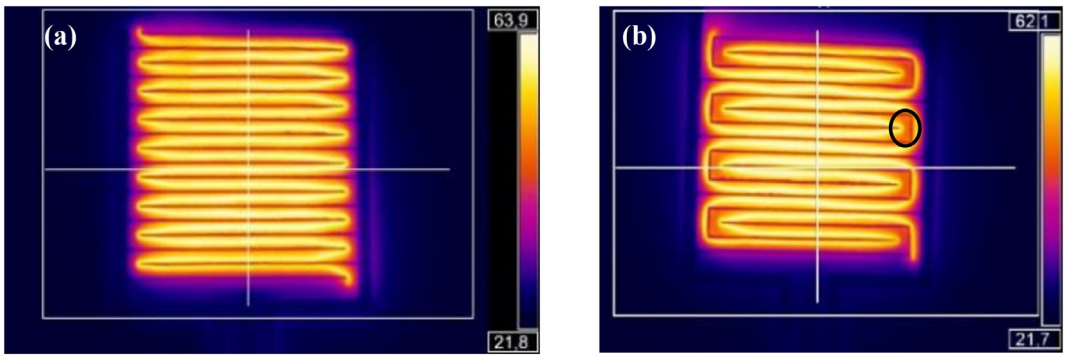



**Fig. 8.** (a) Thermograph image at 24 V of ECI 8001 ink (self-limiting T 65 °C) with 4COMB configuration and (b) 4SNAKE configuration where one of the areas showing temperature gradient within the heating area is highlighted in black.

### 3.3. Hybrid system prototype

A first aluminum prototype was developed and tested (-10 °C). In order to check if the 40 °C self-limiting heater can reach target temperature (6–10 °C) at an environment of −10 °C, the heater was printed on a SHP aluminum sheet, with the silver electrodes printed on the carbon layer in the 4COMB configuration. 24 V were supplied to the sample according to previous results.

Fig. 10(a) shows the temperature measured on the SHP surface of the aluminum sample at room temperature and at −10 °C. While the aluminum at room temperature quickly reached the self-limiting temperature of 40 °C after applying 24 V, the equilibrium temperature reached at chamber conditions (-10 °C) is approximately 15 °C.

Fig. 10(b) shows an image of the reference and hybrid samples under test conditions. It is observed that ice is formed on the reference sample, bare aluminum and SHP surface with no heating (right side), but no ice is observed on the hybrid prototype on none of the SHP or Bare Al surfaces (left side). Additionally, complete water removal is observed in the SHP aluminum surface while some water drops can still be observed on the Bare Al, which could act as nuclei for refreezing of the surface or run-back water on adjacent surfaces. The power consumption calculated for the system is 5.69 W, leading to an energy consumption of 0.702 kW/m2 under test conditions for the SHP surface to completely remove water. In the case of bare aluminum, the evaporation temperature needs to be reached for complete water removal from the surface leading to higher energy consumption. Results show that the stud-

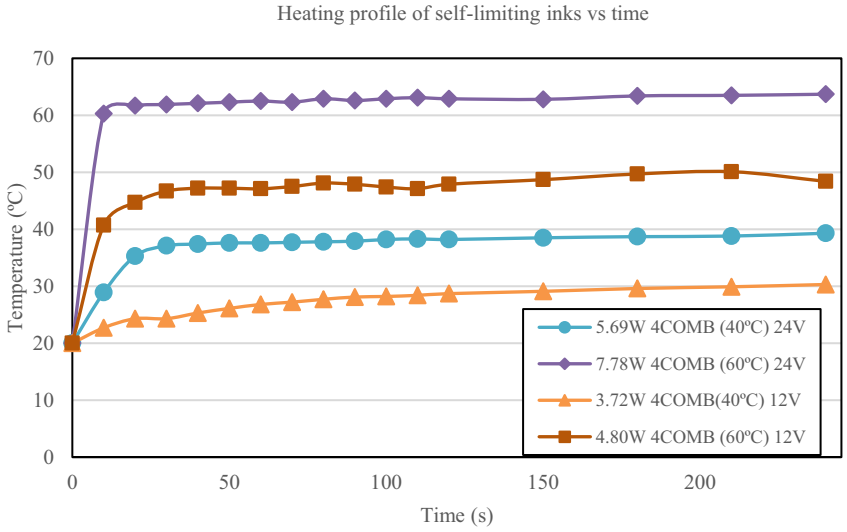



**Fig. 9.** Heating profile of the 4COMB configuration for the two self-limiting PTC inks at 12 V and 24 V.

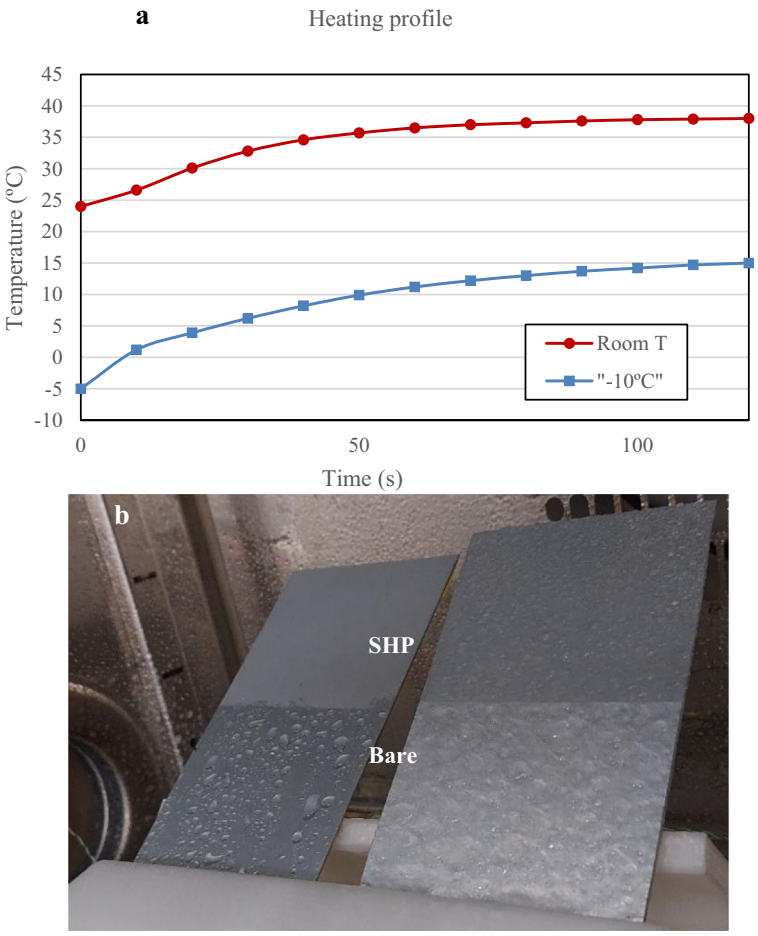



**Fig. 10.** (a) Heating profile of aluminum prototype at room temperature and at −10 °C; (b) Image of reference sample and the hybrid prototype on the left side.

ied hybrid system could lead to a complete anti-icing surface combining SHP and the PTC based heating system with a lower power consumption than a merely heating system.

## 4. Conclusions

In this work we have fabricated an anti-icing system combining SHP and a self-limiting printed heating element to be used at −10 °C environment.

SHP surface combined with 40 °C self-limiting PTC carbon ink based heater show an efficient anti-icing performance with complete water removal from the surface. From our study an energy consumption of 0.702 kW/m$^2$ is required for the system to maintain the SHP surface water/ice free at −10 °C.

This prototype is a proof of concept to demonstrate that SHP and printed self-limiting heaters based on PTC inks can be used for anti-icing hybrid systems. Other configurations are being studied. The performance of the system will be further evaluated under different environmental conditions.

## CRediT authorship contribution statement

**Olatz Adarraga:** Conceptualization, Investigation, Writing – original draft, Writing – review & editing, Visualization. **Celina Vaquero:** Conceptualization, Investigation, Writing – original draft, Writing – review & editing, Visualization. **Leire Bilbao:** Conceptualization, Investigation, Resources. **Jon Maudes:** Conceptualization, Resources. **Ana Perez:** Conceptualization, Resources. **Haizea Villaverde:** Conceptualization, Resources. **Izaskun Bustero:** Funding acquisition, Writing – original draft, Visualization, Writing – review & editing, Supervision. **Ibai Santamaría:** Writing – review & editing. **Marie Pervier:** Investigation, Writing – review & editing.

## Data availability

Data will be made available on request.

## Declaration of Competing Interest

The authors declare that they have no known competing financial interests or personal relationships that could have appeared to influence the work reported in this paper.

## Acknowledgements

We thank Dr Isabel Obieta for useful contribution. This work was partially supported by the Basque Government (Elkartek KK--2021/00040) and (Elkartek KK-2021/00066). This project also received funding from the Clean Sky 2 Joint Undertaking (CSJU) under grant agreement No. 821301. The JU received support from the European Unioń s Horizon 2020 (H2020) research and innovation program and the Clean Sky 2 JU members other than the Union.

## References

[1] O. Meier, A Handbook Method for the Estimation of Power Requirements for Electrical De-Icing Systems Department Fahrzeugtechnik Und Flugzeugbau Projekt Verfasser: Oliver Meier (2010).
[2] L. Vertuccio, F. De Santis, R. Pantani, K. Lafdi, L. Guadagno, Compos B Eng vol. 162 (2019) pp. 600–610.
[3] M.J. Kreder, J. Alvarenga, P. Kim, J. Aizenberg, Nat. Rev. Mater. 1 (2016).
[4] X. Zhou, Y. Sun, J. Liu, X. Zhou, Y. Sun, J. Liu, Adv. Mater. Interfaces 8 (2021) 2100327.
[5] Z. Zhao, H. Chen, X. Liu, Z. Wang, Y. Zhu, Y. Zhou, Surf. Coat. Technol. 404 (2020).
[6] L. Gao, Y. Liu, L. Ma, H. Hu, Renew. Energy 140 (2019) 943–956.
[7] C. Antonini, M. Innocenti, T. Horn, M. Marengo, A. Amirfazli, Cold Reg. Sci. Technol. 67 (2011) 58–67.
[8] Z. Zhao, H. Chen, X. Liu, H. Liu, D. Zhang, Surf. Coat. Technol. 349 (2018) 340–346.
[9] ML.A. Pervier, D.W. Hammond, Engineering Fracture Mechanics, 214 (2019) 223-232.
[10] O. Adarraga, C. Agustín-Sáenz, I. Bustero, F. Brusciotti, Sci. Rep. 13 (2023) 1737.
[11] K. Seo, M. Kim, J.K. Ahn, D.H. Kim, Korean J. Chem. Eng. 32 (2015) 2394–2399.
[12] V. Hejazi, K. Sobolev, M. Nosonovsky, Sci. Rep. 3 (2013).
[13] K.A. Emelyanenko, A.M. Emelyanenko, L.B. Boinovich, Coatings vol. 10 (2020) p. 648.



https://dspace.org/

# Anti-icing solutions combining printed electronics and nanotexturing of Al alloys

**Adarraga, Olatz; Vaquero, Celina; Bilbao, Leire; Maudes, Jon; Pérez-Márquez, Ana ...**

**2023-12-03**
Elsevier
https://doi.org/10.1016/j.matpr.2023.05.337
Adarraga O, Vaquero C, Bilbao L, et al., (2023) Anti-icing solutions combining printed electronics and nanotexturing of Al alloys. Materials Today: Proceedings, Volume 93, Part 1, pp. 24-30

Downloaded from a DSpace repository. https://dspace.org/